CONVERGENCE OF THE LERAY α-REGULARIZATION SCHEME FOR DISCONTINUOUS SOLUTIONS OF THE INVISCID BURGER'S EQUATION.

YEKATERINA PAVLOVA 49744421

ADVISORS: JOHN LOWENGRUB.

EDRISS TITI.

PHYSICAL SCIENCE: MATHEMATICS.

ABSTRACT.

Title: Convergence of the Leray α-Regularization Scheme for Discontinuous Solutions of the Inviscid Burger's Equation.

Author: Yekaterina Sergeyevna Pavlova.

Faculty Mentors: John Lowengrub, Edriss Titi.

In this paper we explore the use of the Leray α-regularization applied to Burger's equation. In the regularization, an additional variable is introduced which is a smoothed version of the original variable and a vector system for the original and smoothed variable is solved simultaneously. We employ a hybrid algorithm combining a centered finite difference scheme for Burger's equation and a spectral method for the regularization. A parameter θ is introduced in order to conserve particular quantities associated with the solution of the regularized problem. For several values of θ, we compare the exact solutions to those of the regularized problem and investigate the dependence of the solutions on the regularization parameter α and on the mesh size. In particular, it is shown that under appropriate conditions and particular values of θ, the numerical Leray α-regularization scheme produces an approximate solution that appears to converge to the unique discontinuous (entropy) solution as the mesh size $h \to 0$ provided that the regularization parameter α and h are related to each other in a precise way. Interestingly, our results suggest that it is only the smoothed variable which converges to the entropy solution.

Key Terms: Burgers Equation, α-Regularization, Leray-α, Entropy Condition, Numerical Partial Differential Equations, Finite Difference Schemes.

1. INTRODUCTION AND BACKGROUND

The numerical solution of conservation laws is critical to understanding nonlinear phenomena in mathematical physics. The prime difficulty in computing conservation laws is that discontinuities develop in the solution. This in many cases necessitates the use of a particular regularization scheme in order to obtain a unique physical solution. In this paper we explore new techniques for solving such equations by focusing on a specific model problem- Burgers equation. Burgers equation is one of the simplest and most well studied nonlinear hyperbolic partial differential equations as it serves as a model for more general conservation laws governing the evolution of mass, momentum and energy. Examples range from shock waves in supersonic wind tunnels to traffic flow (Knobel, 2000). Burgers equation is a special case of a general conservation law:

$$u_t + f(u)_x = 0, \tag{1}$$

where $u(x,t)$ is the amount of a conserved quantity such as density, momentum or internal energy and $f(u)$ describes the flux of the conserved quantity, in the case of Burgers equation, $f(u) = \frac{1}{2}u^2$. The inviscid form of Burgers equation that is to be considered here is given by:

$$u_t + uu_x = 0 \quad x \in \Re,\ t > 0, \tag{2}$$

together with periodic (period $T = 1$) initial conditions:

$$u(x,0) = \varphi(x) = \varphi(x+T) \quad x \in \Re. \tag{3}$$

Assuming that no discontinuities develop in time, the solution $u(x,t)$ can be obtained by the method of characteristics in the same way as for the linear advection equation $u_t + cu_x = 0$, except here the characteristic speed is no longer constant(Knobel 135). The solution $u(x,t)$ is constant along the characteristic curves which, for Burger's equation, are given by:

$$x(t) = \varphi(x_o)t + x_0. \tag{4}$$

The solution $u(x,t)$ is then given by:

$$u(x,t) = \varphi(x_o), \tag{5}$$

where x_o is a zero of the function

$$0 = G(x_o) = x - \varphi(x_o)t - x_0, \tag{6}$$

(e.g. see Strauss 361). If $\frac{d\varphi(x_o)}{dx_o} \geq 0$, then this equation is uniquely solvable for all t. In this case, the solution is an expansion fan or is a constant in the case of equality. The characteristics do not intersect, so unless initial conditions are discontinuous, the solution $u(x,t)$ will remain smooth for all times. However if $\frac{d\varphi(x_o)}{dx_o} < 0$ for some x_o in the initial periodic profile then equation (6) may not be uniquely solvable for x_o. As a consequence some of the characteristics intersect resulting in discontinuities and non-differentiability of the solution. However it is still possible to obtain the solution in the weak (or integral) sense (LeVeque 27). Such solutions typically are piecewise smooth. In the case of a single discontinuity, let $(x_s(t), t)$ be a curve in the $x-t$ plane across which $u(x,t)$ is discontinuous. Then the velocity of the curve is given by the Rankine-Hugoniot condition (Knobel 134):

$$\dot{x}_s(t) = \frac{f(u^+) - f(u^-)}{u^+ - u^-} = \frac{1}{2}(u^+ + u^-). \tag{7}$$

The discontinuity in the solution is called a shock wave, $\dot{x_s}(t)$ is the speed of propagation, $u^+ = \lim_{x \to +x_s} u(x,t)$ and $u^- = \lim_{x \to -x_s} u(x,t)$ are right and left limits that will in general not be equal across the shock wave creating an infinite spatial gradient of $u(x,t)$. If the shock is not present initially, the time of formation is calculated as the smallest time when $u_x(x,t)$ becomes infinite which is given by (Knobel 143):

$$t_b = \min_{x_o} \frac{-1}{\frac{d}{dx_o}\varphi(x_o)}. \tag{8}$$

Lastly, in order to ensure uniqueness of the weak solution, the entropy condition is used as the physical selection mechanism. That is, the speed of the wave just behind the shock must be higher than the speed just ahead of it (Strauss 366). The entropy condition guarantees (in analogy with gas dynamics) that the entropy of material increases as it passes the discontinuity, this can be written as:

$$u^- > \dot{x}_s(t) > u^+, \tag{9}$$

for Burger's equation. Hence the solution that satisfies the entropy condition is a unique physical solution. A more convenient method to test if the entropy condition is satisfied is the Oleinik inequality (Knobel 183):

$$\frac{u(x+a,t)-u(x,t)}{a} < \frac{C}{t}, \tag{10}$$

which holds $\forall\ a,t > 0$ and some constant C that depends only on the initial conditions $u(x,0) = \varphi(x)$. This condition restricts how large the positive secant slopes of $u(x)$ can become in time, while the negative slopes remain unrestricted (Knobel 183).

2. LERAY-α REGULARISATION PROBLEM STATEMENT AND CONSERVED QUANTITIES

Although many methods of approximation of solutions to conservation laws exist (Iserles, 1996; LeVeque, 1992), the purpose of this research is to test numerically several versions of the Leray-α regularization scheme. A version of this regularization was originally derived by Leray for the Navier-Stokes equations governing incompressible fluid flow (Leray, 1936). Here, we introduce another parameter θ, with $0 \leq \theta \leq 1$, and we consider:

$$v_t^\alpha + \theta u^\alpha v_x^\alpha + (1-\theta) u_x^\alpha v^\alpha = 0 \tag{11}$$

where v^α is related to u^α by:

$$v^\alpha = H[u^\alpha] \equiv u^\alpha - \alpha^2 u_{xx}^\alpha \tag{12}$$

with initial data:

$$v^\alpha(x,0) = v_o^\alpha(x) = \varphi(x) = \varphi(x+T) \tag{13}$$

For the case $\theta = 1$, this regularization scheme was previously proposed and studied by H. Bhat (Bhat, 2005) and E.Tadmor et al. (Tadmor et al., 2006). However in those works, the numerical investigations did not conclusively demonstrate the convergence properties of the proposed scheme. In this paper, the convergence of functions $u^\alpha(x,t)$ and $v^\alpha(x,t)$ to the exact entropy solution $u(x,t)$ of the inviscid Burgers equation (2) is studied numerically as $\alpha \to 0$. If $\alpha = 0$ we have $v^\alpha = u^\alpha$ and the regularization problem becomes (2). It should be noted that both functions $u^\alpha(x,t)$ and $v^\alpha(x,t)$ are smooth and do not have discontinuities, however in the limit as $\alpha \to 0$ there is recent evidence that solutions for $\theta = 1$ converge to possibly discontinuous entropy solutions of Burgers equation(Tadmor et al.,2006).

We note that other α-regularization models exist including the Navier-Stokes-α (NS-α), the Magnetohydrodynamic-α (MHD-α) and the Lagrangian Averaged NS(or MHD)-α (LANS-α, LAMHD-α). Such models modify the original equations by making nonlinearities milder, which leads to smoother solutions without unnecessary energy dissipation in the system (Linshiz and Titi, 2006).

If $\theta = 1$ the system $(11) - (12)$ becomes:

$$v_t^\alpha + u^\alpha v_x^\alpha = 0 \tag{14}$$

$$v^\alpha = u^\alpha - \alpha^2 u_{xx}^\alpha$$

Define the L_1 norm by

$$\|v\|_{L_1} \equiv \int_0^T |v|\, dx. \tag{15}$$

Then, it can be shown that the maximum of $v^\alpha(x,t)$ in (14) is conserved. In fact given smooth enough functions, it has been proven (Tadmor et al., 2006) that:

$$\|v^\alpha(.,t)\|_{L_1} \leq \|\varphi(x_o)\|_{L_1} \leq Const. \tag{16}$$

The parameter θ can be chosen such that certain quantities are exactly conserved by the equation (11). The conserved quantities for $\theta = 1, \frac{1}{3}, \frac{2}{3}$ are stated in the following theorems (2),(3) and (4).

Theorem 1. ***($\theta = 1$).*** *Consider (14) and assume that u^α and v^α are periodic with period T, then:*

$$\int_0^T v^\alpha dx = constant. \tag{17}$$

That is, the mass is conserved. Furthermore, $max_x v^\alpha(x,t)$ is conserved in time.

Proof. Integrate (14) by parts and apply boundary conditions:

$$\int_0^T v_t^\alpha + u^\alpha v_x^\alpha dx = 0$$

$$\frac{\partial}{\partial t}\int_0^T v^\alpha dx + \int_0^T u^\alpha v_x^\alpha dx = 0$$

$$\frac{\partial}{\partial t}\int_0^T v^\alpha dx - \int_0^T u_x^\alpha v^\alpha dx = 0 \tag{18}$$

Use (12) to simplify (18):

$$\frac{\partial}{\partial t}\int_0^T v^\alpha dx - \int_0^T u_x^\alpha (u^\alpha - \alpha^2 u_{xx}^\alpha)dx = 0$$

$$\frac{\partial}{\partial t}\int_0^T v^\alpha dx - \int_0^T \frac{1}{2}((u^\alpha)^2)_x - \frac{\alpha^2}{2}((u_x^\alpha)^2)_x dx = 0$$

Applying boundary conditions, the second integral vanishes and we have:

$$\frac{\partial}{\partial t}\int_0^T v^\alpha dx = 0 \tag{19}$$

that is:

$$\int_0^T v^\alpha dx = constant$$

To show that the maximum of v^α is conserved in time, let $\tilde{x}(t)$ be a point where maximum occurs, then:

$$v_t^\alpha(\tilde{x}(t),t) + u^\alpha(\tilde{x}(t),t)v_x^\alpha(\tilde{x}(t),t) = 0$$

Since $v_x^\alpha(\tilde{x}(t),t) = 0$ at the point of maximum, we have $v_t^\alpha + u^\alpha \cdot 0 = 0$ and $v^\alpha(\tilde{x}(t),t) = const$, that is $max_x v^\alpha$ remains constant in time.

□

For $\theta = \frac{1}{3}$, the system $(11) - (12)$ becomes:

$$v_t^\alpha + \frac{1}{3}u^\alpha v_x^\alpha + \frac{2}{3}v^\alpha u_x^\alpha = 0 \tag{20}$$

$$v^\alpha = u^\alpha - \alpha^2 u_{xx}^\alpha$$

Theorem 2. ***($\theta = \frac{1}{3}$).*** *Consider (20) and assume that u^α and v^α are periodic with period T, then:*

$$\int_0^T (u^\alpha)^2 + \alpha^2 (u_x^\alpha)^2 dx = constant \tag{21}$$

That is, a modified energy is conserved.

Proof. Multiply (20) by u^α and integrate:

$$\int_0^T u^\alpha v_t^\alpha dx + \frac{1}{3}\int_0^T (u^\alpha)^2 v_x^\alpha dx + \frac{2}{3}\int_0^T v^\alpha u^\alpha u_x^\alpha dx = 0$$

$$\int_0^T u^\alpha v_t^\alpha dx + \frac{1}{3}(\int_0^T (u^\alpha)^2 v_x^\alpha + v^\alpha((u^\alpha)^2)_x dx) = 0$$

$$\int_0^T u^\alpha v_t^\alpha dx + \frac{1}{3}(\int_0^T ((u^\alpha)^2 v^\alpha)_x dx) = 0$$

Applying boundary conditions, the last term is zero and we obtain:

$$\int_0^T u^\alpha v_t^\alpha dx = 0 \tag{22}$$

Plug (12) in to (22) and we have:

$$\int_0^T u^\alpha v_t^\alpha dx = \int_0^T u^\alpha (u_t^\alpha - \alpha^2 u_{xxt}^\alpha) dx = \frac{1}{2}\frac{\partial}{\partial t}\int_0^T (u^\alpha)^2 + \alpha^2 (u_x^\alpha)^2 dx = 0$$

that is:

$$\int_0^T (u^\alpha)^2 + \alpha^2 (u_x^\alpha)^2 dx = constant$$

□

For $\theta = \frac{2}{3}$, the system $(11) - (12)$ becomes:

$$v_t^\alpha + \frac{2}{3} u^\alpha v_x^\alpha + \frac{1}{3} v^\alpha u_x^\alpha = 0 \tag{23}$$

$$v^\alpha = u^\alpha - \alpha^2 u_{xx}^\alpha$$

Theorem 3. ***($\theta = \frac{2}{3}$).*** *Consider* (23) *and assume that* u^α *and* v^α *are periodic with period* T*, then:*

$$\int_0^T |v^\alpha|^2 \, dx = constant. \tag{24}$$

That is, the energy is conserved.

Proof. Multiply (23) by v^α and integrate:

$$\int_0^T v^\alpha v_t^\alpha dx + \frac{2}{3}\int_0^T v^\alpha u^\alpha v_x^\alpha dx + \frac{1}{3}\int_0^T (v^\alpha)^2 u_x^\alpha dx = 0$$

$$\frac{1}{2}\int_0^T (v_t^\alpha)^2 dx + \frac{1}{3}\int_0^T (u^\alpha (v^\alpha)^2)_x dx = 0$$

Applying boundary conditions, the last term is zero and we obtain:

$$\frac{1}{2}\frac{d}{dt}\int_0^T |v^\alpha|^2 \, dx = 0 \tag{25}$$

$$\int_0^T |v^\alpha|^2 \, dx = constant$$

□

3. NUMERICAL IMPLEMENTATION

Consider the problem $(11) - (13)$ with periodic (of period T=1) initial conditions $v^\alpha(x,0) = v_o(x) = v_o(x+T)$. Create a fine mesh on the interval $[0,1]$ such that $0 = x_0 < x_1(= h) < x_2(= 2h) < ... < x_N(= Nh) = 1$, where N and h are the number and size of the step in space respectively. Two initial profiles are considered to test the behavior of numerical solution:

(26) $$v_o(x) = 1 - cos(2\pi x),$$

and

(27) $$v_o(x) = cos(2\pi x).$$

In the former, the solution remains nonnegative and the shock moves; while in the latter, the solution has both positive and negative parts and the shock is stationary. The solution is computed up to a time t_f. Time is discretized as $0 = t_0 < t_1(= \Delta t) < t_2(= 2\Delta t) < ... < K\Delta t = t_f$, where K and Δt are the number and size of time steps respectively. In particular $t_f = t_b, \frac{3}{2}t_b$ and $2t_b$ are considered, where t_b is the time at which the discontinuity forms and is given by equation (8). With this discretization define $u_j^n = u(x_j, t_n)$ and $v_j^n = v(x_j, t_n)$.

Equations (11) and (12) are solved simultaneously as a coupled system. Starting with initial conditions $v_o(x) = \varphi(x)$, evaluated at the mesh points, the values of $u_j^0 = u(x_j, 0)$, $j = 0, ..., N$ are obtained from (12) by means of Finite Fourier Transform. Then at the first time step, $v_j^1 = v(x_j, \Delta t)$ is computed from equation (11) using the Forward Time Centered Space (FTCS) spatial discretization scheme. However this method is actually unstable for use at long times and so the further time steps are computed using second order multistep Leap Frog scheme (Strikwerda, 2004). The solution is computed by going back and forth between equations (11) and (12) at each time step.

3.0.1. ***Solution to*** $u - \alpha^2 u_{xx} = v$ ***at each time step.*** Several methods could be used to compute $u(x, t_n)$ given $v(x, t_n)$ for each fixed t_n from (12) such as the Thomas algorithm (Strikwerda 88) applied to finite

difference methods (Thomas,1995), and the spectral method based on the Finite/Fast Fourier Transform (Strikwerda 46). Here we use a spectral method where the Complex Split Radix Fast Fourier Transform (FFT) subroutine (Kifowit, 2005) was used to implement the Finite Fourier Transform. This approach gives a smaller maximum L_1 error compared to the Finite Difference algorithm using the Thomas solution method. The forward Finite Fourier Transform is defined as:

$$\hat{u}_k = \sum_{j=0}^{N-1} u_j e^{-2ijk\pi h}, \tag{28}$$

and the backward Finite Fourier Transform is given by:

$$u_j = h \sum_{k=0}^{N-1} \hat{u}_k e^{2ijk\pi h}. \tag{29}$$

Given $v(x,t_n)$ at the mesh points for a fixed time, the forward transform gives an array $\hat{v}_k, k = 0, ..., N-1$. Using the derivative formula for the Finite Fourier transform and shifting indices, equation (12) becomes:

$$\sum_{k=0}^{N-1} \hat{v}_k e^{2ij(k-N/2)\pi h} = \sum_{k=0}^{N-1} \hat{u}_k e^{2ij(k-N/2)\pi h} + \sum_{k=0}^{N-1} 4(\alpha(k-N/2)\pi)^2 \hat{u}_k e^{2ij(k-N/2)\pi h}.$$

Matching coefficients, this gives $\hat{u}_k$ in terms of known quantities (Thomas 101):

$$\hat{u}_k = \frac{\hat{v}_k}{1 + 4\alpha^2\pi^2(k-N/2)^2}, \quad k = 0, ..., N-1. \tag{30}$$

Then using backward transform (29), $u(x,t_n)$ is obtained for that time step t_n.

Difficulties with this method might arise due to the occurrence of aliasing instabilities over long time for large N (Boyd, 2001). In this case some smoothing of the high modes of the Fourier spectrum is required. Aliasing instability here is controlled by using $25th$ order Fourier filtering to damp the highest modes (Hou et al., 1994):

$$\Pi\left[\hat{v_k}\right] = e^{-10(|k|/N)^{25}} \hat{v_k}. \tag{31}$$

The overall accuracy of the method is determined by the filter and is of order $O((1/N)^{25})$ (Hou et al.,1994). To reduce the noise introduced by taking derivatives, Krasny filtering was also used, where the Fourier modes of magnitude less than the tolerance level $\epsilon = 10E-12$ were set to zero (Krasny, 1986). The

combination of both methods, when applied to $\hat{v_k}$ before evaluating $\hat{u_k}$ from (30), significantly improves the accuracy of the method.

3.0.2. ***First Time Step FTCS (Forward Time Centered Space) Scheme.*** In this scheme forward and center difference formulas are used to discretise time and space derivatives respectively (Strikwerda 17):

$$\frac{d}{dt}v_j^n = \frac{v_j^{n+1} - v_j^n}{\Delta t} + O(\Delta t) \approx \frac{v_j^{n+1} - v_j^n}{\Delta t}, \tag{32}$$

$$\frac{d}{dx}u_j^n = \frac{u_{j+1}^n - u_{j-1}^n}{2h} + O(h^2) \approx \frac{u_{j+1}^n - u_{j-1}^n}{2h}. \tag{33}$$

Using (32) and (33), equation (11) becomes:

$$\frac{v_j^1 - v_j^0}{\Delta t} + \theta u_j^0(\frac{v_{j+1}^0 - v_{j-1}^0}{2h}) + (1-\theta)v_j^0(\frac{u_{j+1}^0 - u_{j-1}^0}{2h}) = O(\Delta t) + O(h^2)$$

which solving for v_j^1 gives:

$$v_j^1 = v_j^0 - \frac{\Delta t}{2h}(\theta u_j^0(v_{j+1}^0 - v_{j-1}^0) + (1-\theta)v_j^0(u_{j+1}^0 - u_{j-1}^0)) + (O(\Delta t) + O(h^2)). \tag{34}$$

Knowing v_j^0 and u_j^0, equation (34) gives v_j^1 for the next time iteration $\forall j = 0, 1, ..., N$. This scheme is used on the first time step only to provide enough information for employing the multistep Leap Frog scheme for the remaining time steps.

3.0.3. ***Time Steps for*** $n > 1$ ***Leap Frog CTCS (Centered Time Centered Space) Scheme.*** In this scheme center difference formulas are used to discretize both time and space derivatives (Strikwerda 17), i.e.:

$$\frac{d}{dt}v_j^n = \frac{v_j^{n+1} - v_j^{n-1}}{2\Delta t} + O(\Delta t^2) \approx \frac{v_j^{n+1} - v_j^{n-1}}{2\Delta t}. \tag{35}$$

Using (35) and (33), equation (11) becomes:

$$\frac{v_j^{n+1} - v_j^{n-1}}{2\Delta t} + \theta u_j^n(\frac{v_{j+1}^n - v_{j-1}^n}{2h}) + (1-\theta)v_j^n(\frac{u_{j+1}^n - u_{j-1}^n}{2h}) = O(\Delta t^2) + O(h^2)$$

which solving for v_j^{n+1} gives:

$$v_j^{n+1} = v_j^{n-1} - \frac{\Delta t}{h}(\theta u_j^n(v_{j+1}^n - v_{j-1}^n) + (1-\theta)v_j^n(u_{j+1}^n - u_{j-1}^n)) + (O(\Delta t^2) + O(h^2)). \tag{36}$$

Therefore, knowing v_j^n, u_j^n and v_j^{n-1}, equation (36) gives v_j^{n+1} for the next time iteration $\forall j = 0, 1, ..., N$.

3.0.4. ***Stability and Convergence.*** For an explicit numerical scheme one of the necessary stability conditions is Courant-Friedrichs-Lewy condition (Strikwerda 34) stating that the ratio $\frac{\Delta t}{h}$ should be held constant and less than one. Physically this means that the solution (e.g. shock wave) can not propagate more than one grid spacing in a single time step. Here, the following stability relation was used:

$$\Delta t = \frac{h}{2}. \tag{37}$$

Since the parameter α is a key convergence parameter, we use the following criteria to determine physically reasonable choices of α. For example, when $\theta = 1$, Theorem 2 states that the maximum of $v^{\alpha}(x,t)$ is conserved in time and thus cannot exceed the maximum in the initial data. However, for a fixed number of partition intervals N considered, there is a particular value of α below which $v^{\alpha}(x)$ becomes oscillatory, hence violating maximum conservation condition. One of the tasks of this numerical investigation was to establish a relation between α and the mesh size that preserves stability and consistency with Theorems $1-4$. For the case $\theta = 1$, holding N fixed, α is decreased incrementally while the maximum of the numerical approximation of $v^{\alpha}(x,t)$ lies within a specified tolerance level δ of the maximum of the initial data. That is, α can only be decreased as long as the following condition holds:

$$|max_{j=1,\ldots,N}\,|v(x_j,t_n)| - (max_{j=1,\ldots,N}\,|\varphi(x_j)|)| \leq \delta, \tag{38}$$

for all discrete times $t_m \leq t_f$.

For the remaining cases $\theta = \frac{1}{3}$ and $\theta = \frac{2}{3}$ the maximum of $v^{\alpha}(x,t)$ need not be conserved and the stopping criteria for decreasing α relies on the results of Theorems 3 and 4. The conserved quantities (21) and (24) are computed numerically for $\theta = \frac{1}{3}$ and $\theta = \frac{2}{3}$ respectively. Using the derivative approximation (33) they become:

$$h\left(\sum_{j=1}^{N}(u_j^n)^2 + \alpha^2(\frac{u_{j+1}^n - u_{j-1}^n}{2h})^2\right) = const \tag{39}$$

and

$$h\left(\sum_{j=1}^{N}\left|v_j^n\right|^2\right) = const. \tag{40}$$

Holding N fixed, α is decreased incrementally while the numerical approximation of the conserved quantity (39) or (40) (depending on θ) lies within a specified tolerance level δ of the initial value $\forall t_n \leq t_f$. That is, α can only be decreased as long as the numerical equivalents of Theorems 3 and 4 are satisfied.

3.1. **Exact Solution.** The numerically computed solution is compared to the exact entropy solution obtained by the method of characteristics for two different initial data (26) and (27).

The discontinuity is calculated from (8) to occur at $t_b = \frac{1}{2\pi}$ for both cases. For $t < t_b$ and $x \in [0,1]$ the continuous solution is found in the same way for both (26) and (27) using equations (4) and (5) and applying Newton's iteration method. The initial guess is randomly chosen in the interval $[0,1]$ and the iteration is repeated until x_o converges to an element of $[0,1]$. However after the break time a different approach must be used because the characteristics intersect (shock formation).

In case of the initial data given in equation (26) the shock forms at $(x_b, t_b) = (\frac{2+3\pi}{4\pi}, \frac{1}{2\pi})$ and the characteristic that initiates the shock originates from $x_o^b = \frac{3}{4}$. Suppose at the break time the speed of the shock, given by (7), is $\dot{x}_s(t_b) \approx \frac{1}{2}(\varphi(x_o^b) + \varphi(x_o^b)) = 1$. At the later times the position of the shock is computed as:

$$x_s(t_b + \Delta tk) = x_b + (\Delta x)_1 + ... + (\Delta x)_k \tag{41}$$

where

$$(\Delta x)_k = \dot{x_s}(t_b + \Delta t(k-1))\Delta t + O(\Delta t^2) \tag{42}$$

and from Rankine-Hugoniot condition (7):

$$\dot{x_s}(t_b + \Delta t(k-1)) = \frac{1}{2}(u^+(t_b + \Delta t(k-1)) + u^-(t_b + \Delta t(k-1))). \tag{43}$$

Knowing the position of the shock at each time step allows for the successful choice of the initial guess in the Newton iteration algorithm when solving equation (4) for x_o. Characteristics starting to the right of x_o^b carry the values of $u(x, t_b + \Delta tk)$ only for x to the right of $x_s(t_b + \Delta tk)$ and the characteristics to the left of x_o^b carry the values of $u(x, t_b + \Delta tk)$ for x to the left of $x_s(t_b + \Delta tk)$.

In the case of the initial data in equation (27) the shock is stationary and is located at $x = \frac{1}{4}$ hence we do not need to use (7) to determine the change in the shock position in time. However, more intervals need

to be considered (i.e., $[-1/4, 1, 4]$, $[1/4, 3/4]$, $[3/4, 5/4]$) for the initial guess generation for the Newton iteration of equation (4) given $(x, t) \in [0, 1] \times [0, t_f]$.

Once the exact entropy solution is obtained, the L_1 error is calculated at each fixed time as:

$$E(t_n)\left[u^\alpha\right] = h \sum_{j=1}^{N} \left|u^\alpha(x_j, t_n) - u_{i,j}\right|, \tag{44}$$

where $u_{i,j}$ is the exact entropy solution computed as described above. The global error is computed as a maximum L_1 error over all times up to t_f:

$$E\left[t_f\right] = max_{n=1,\ldots,K} \left|E(t_n)\right| \tag{45}$$

4. Results and Discussion

4.1. θ**=1.** For the initial data (26) the solution is nonnegative and the nonzero parts of the solution move to the right in time at different speeds, however for the initial data (27) the position of the shock is fixed at $x = \frac{1}{4}$. Figures 1 and 2 show the exact and numerical solution curves superimposed for $v^\alpha(x, t)$ and $u^\alpha(x, t)$ for both initial conditions. Observe that up to time $t = 3/2t_b$, v^α is an excellent approximation of the exact solution. The function u^α also approximates the exact solution but is smoothed over a larger region and deviates more near the discontinuity. At larger times, for example $t = 2t_b$, it is apparent that v^α does not decay while both the exact solution and u^α do decay. This will be important later when we check the Oleinik entropy inequality.

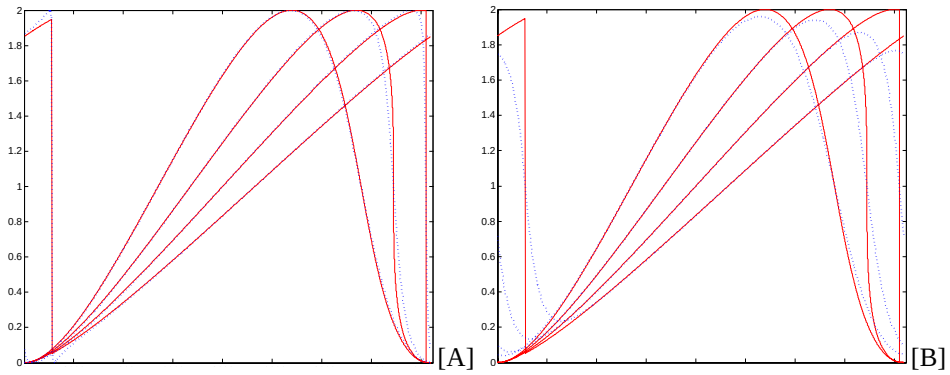

FIGURE 1. Solution curves computed up to $t = 2t_b$ for the initial data (26). Red solid curves represent the exact solution for $t = (1/2)t_b, t_b, (3/2)t_b$ and $2t_b$. Blue dotted curves represent the corresponding numerical solution:[A]-$V^\alpha(x)$,[B]-$U^\alpha(x)$.$N = 16384, \alpha = 0.0327$.

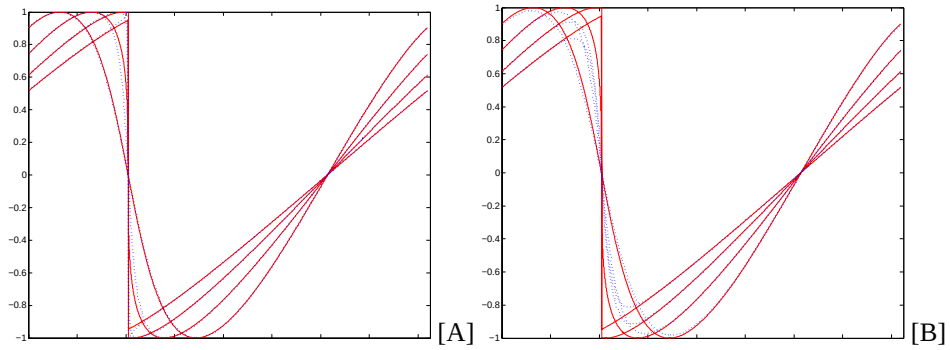

FIGURE 2. Solution curves computed up to $t = 2t_b$ for the initial data (27). Red solid curves represent the exact solution for $t = (1/2)t_b, t_b, (3/2)t_b$ and $2t_b$. Blue dotted curves represent the corresponding numerical solution:[A]-$V^\alpha(x)$,[B]-$U^\alpha(x)$.$N = 16384, \alpha = 0.0216$.

The tolerance level $\delta = 10E - 5$ is used with equation (38) to generate a relationship between α and $N = \frac{1}{h}$ computed up to twice the break time. This relationship is shown on Figure 3 in log-log scale for both initial conditions (26) and (27). The physically meaningful α lie above the curves. For combinations of α and $\frac{1}{h}$ below the curves, oscillations will develop in the numerical solution and the maximum of v^α will no longer be conserved.

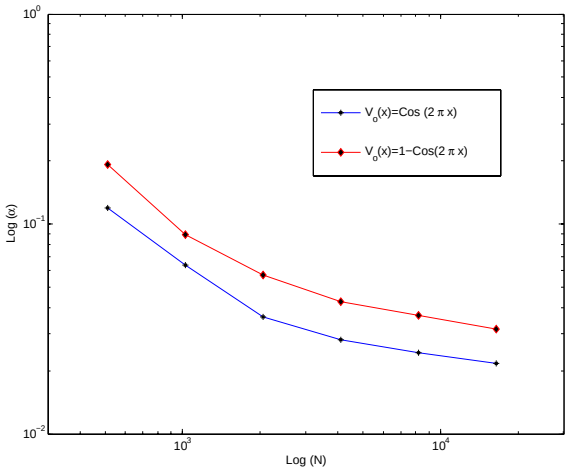

FIGURE 3. Relationship between α and N for $\theta = 1$ computed up to $t = 2t_b$ (twice the break time).

The local L_1 error (44) as well as the global L_1 error (45) were computed. Figure 4 shows the evolution of L_1 error in time for $N = 8192$ for the case of the initial data in (27). The vertical lines mark the times t_b,$\frac{3}{2}t_b$ and $2t_b$. Observe that the maximum error occurs just after the break time. Note that the error for v^α is significantly less than the error for u^α. However, around time $t = 2t_b$, the error in v^α begins to increase in time due to the fact that v^α does not decay.

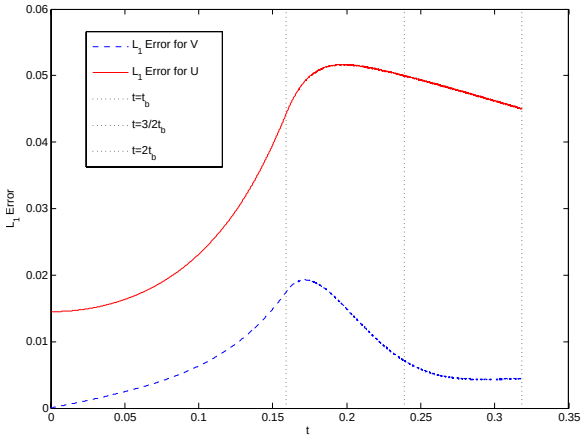

FIGURE 4. Local L_1 Error (44) as a function of time computed for both u^α and v^α up to $t_f = 2t_b$. $N = 8192$, $\alpha = 0.0243$,$V_o(x) = Cos(2\pi x)$.

In Figures 5A and 5B the global error up to $t = \frac{3}{2}t_b$ and $t = 2t_b$, as well as the local error at $t = t_b$, is shown as a function of α for both initial conditions (26) and (27). In all cases the rate of convergence in α is approximately 1 or better for the error in u^α and v^α. The reference lines indicating convergence rates of $p = 1$ (dashed) and $p = 1/2$ (dash-dot) are also shown in Figures 5A and 5B.

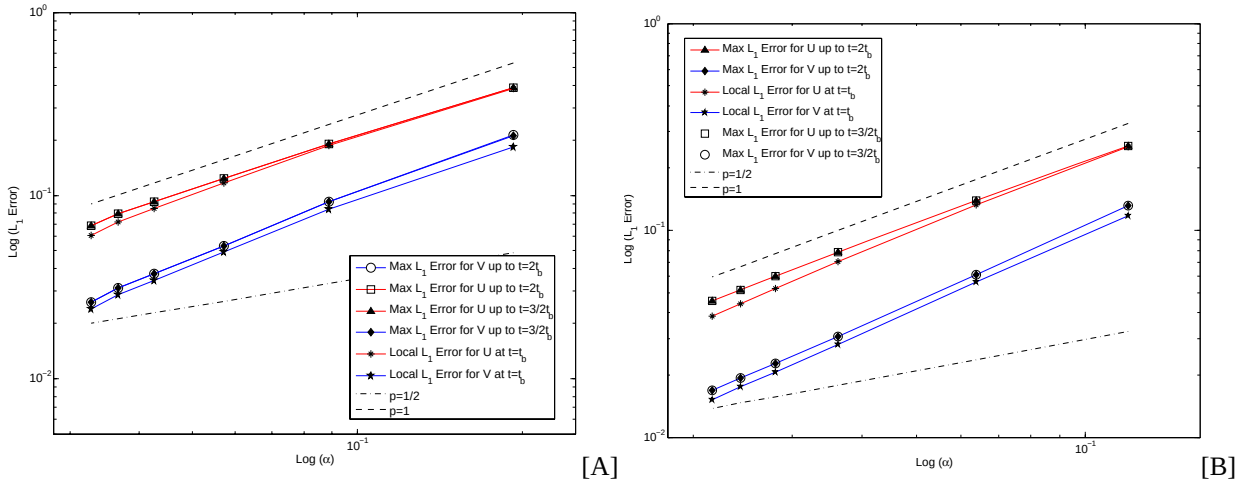

FIGURE 5. [A]: Relationship between global (max) or local L_1 error and α for $\theta = 1$ and initial condition (26). [B]:Relationship between global (max) or local L_1 error and α for $\theta = 1$ and initial condition (27). (The reference slope lines are indicated by $p = 1$ and $p = 1/2$.)

Equation (10) is utilized to check if numerical solution satisfies the entropy condition. The equivalent representation of Oleinik inequality that is easier to check numerically is:

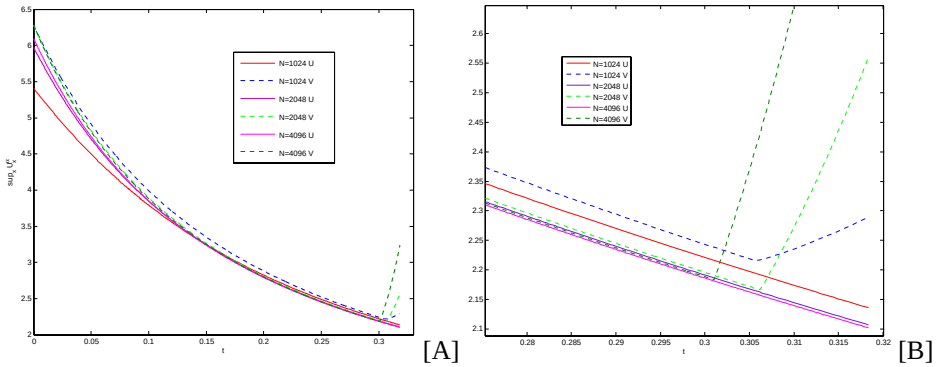

FIGURE 6. [A]:Oleinik Inequality (46) plotted for $\theta = 1$ and initial condition $v_0 = Cos(2\pi x)$,[B]:Zoom in on the area where v^α starts violating the entropy condition.

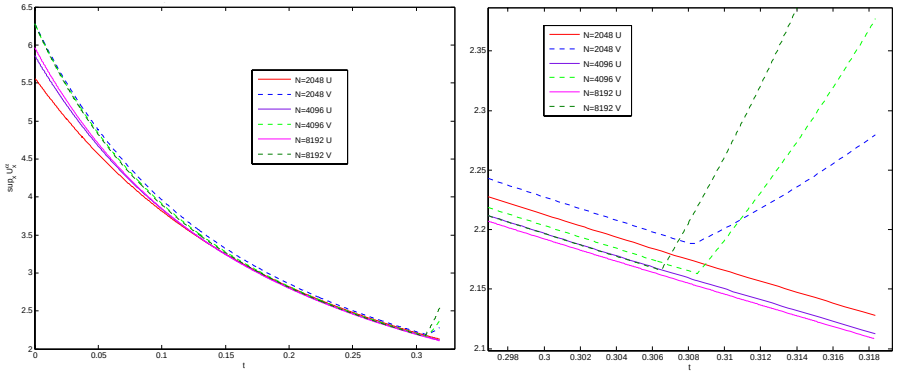

FIGURE 7. [A]:Oleinik Inequality (46) plotted for $\theta = 1$ and initial condition $v_0 = 1 - Cos(2\pi x)$,[B]:Zoom in on the area where v^α starts violating the entropy condition.

(46)
$$\max_{x_i} \frac{v^\alpha(x_{i+1},t) - v^\alpha(x_i,t)}{h} < \frac{C}{t}, \quad i = 0, ..., N-1.$$

Figures 6 and 7 show that the positive slopes are bounded for both types of initial conditions (26) and (27) for $u^\alpha(x,t)$. Therefore it appears that the numerical solution $v^\alpha(x,t)$ does satisfy entropy condition, thus suggesting convergence to the unique physical solution. Interestingly, from Figures 6 and 7 it appears that v^α does not satisfy the Oleinik inequality. Note that as the mesh is refined, the rapid growth in v^α_x occurs earlier in time suggesting that v^α violates Oleinik inequality in the limit $h \to 0$. The general question of convergence of discrete solutions to the continuous entropy solution strongly depends on the choice of numerical scheme. We conjecture that the only appropriate numerical schemes for which v^α converges to the entropy solution are of upwind-type which will yield convergence to the entropy solution as $h \to 0$ even if $\alpha = 0$.

As an additional check of accuracy, (17) was computed numerically at each time step. The difference between (17) at time zero and (17) at any other time step did not exceed $1E-8$, hence implying that the numerical scheme also conserves this quantity.

4.2. $\theta = \frac{2}{3}$**.** We next consider the case in which $\theta = \frac{2}{3}$. Here, the stopping criterion:

$$\left| h\sum_{i=0}^{N-1}(v^{\alpha}(x_i,t_j))^2 - h\sum_{i=0}^{N-1}(v^{\alpha}(x_i,0))^2 \right| \leq \delta \tag{47}$$

is used to determine the range of physically relevant α. Figure 9 shows the numerical solution curves for v^{α} and v^{α} computed using $\theta = \frac{2}{3}$ and α as labeled. Observe that v^{α} has large overshoots near the discontinuity and the function u^{α} provides a better approximation of the exact physically meaningful solution.

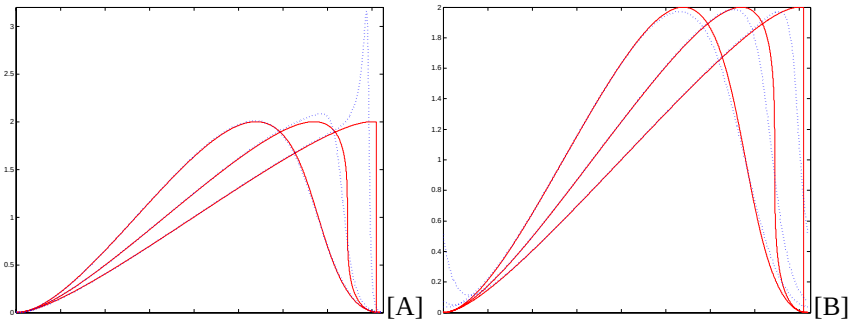
[A] [B]

FIGURE 8. ($\theta = \frac{2}{3}$)Solution curves computed up to $t = \frac{3}{2}t_b$ for the initial data (26). Red solid curves represent the exact solution for $t = (1/2)t_b, t_b, (3/2)t_b$. Blue dotted curves represent the corresponding numerical solution:[A]-$V^{\alpha}(x)$,[B]-$U^{\alpha}(x)$.$N = 16384$,$\alpha = 0.0297$.

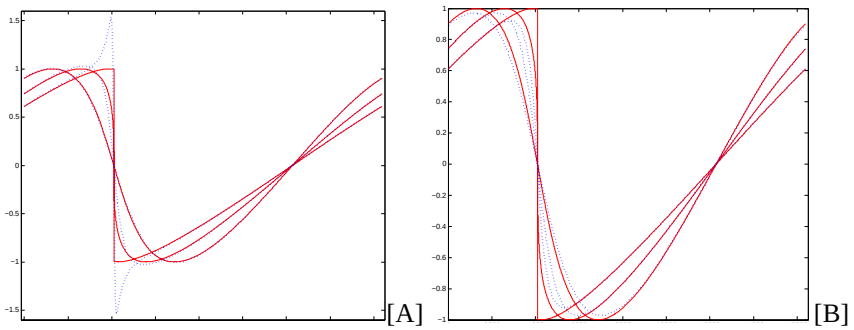
[A] [B]

FIGURE 9. ($\theta = \frac{2}{3}$)Solution curves computed up to $t = \frac{3}{2}t_b$ for the initial data (27). Red solid curves represent the exact solution for $t = (1/2)t_b, t_b, (3/2)t_b$. Blue dotted curves represent the corresponding numerical solution:[A]-$V^{\alpha}(x)$,[B]-$U^{\alpha}(x)$.$N = 16384$,$\alpha = 0.0281$.

The numerical investigation shows that for a given N, the parameter α can not be decreased indefinitely without violating Theorem 3. The relationship between α and N is established as described previously

using (47) with the tolerance level $\delta = 10E-7$. The plot of this relationship is presented in Figure 10. Analogously to the case of $\theta = 1$, the physically meaningful α lie above the curves. For the combinations of α and N below the curves, the energy (40) is not conserved in time to the tolerance level specified above, thus violating Theorem 4 and therefore not providing a valid solution to the modeled problem.

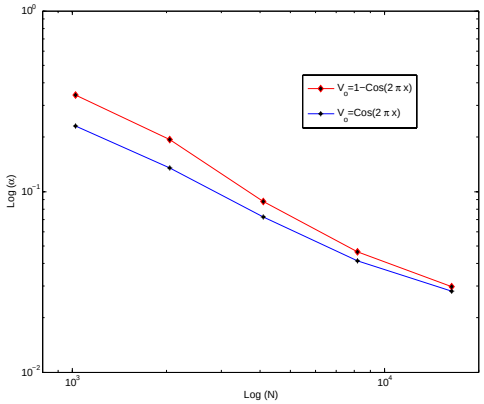

FIGURE 10. Relationship between α and N for $\theta = \frac{2}{3}$ computed up to $\frac{3}{2}$ break time.

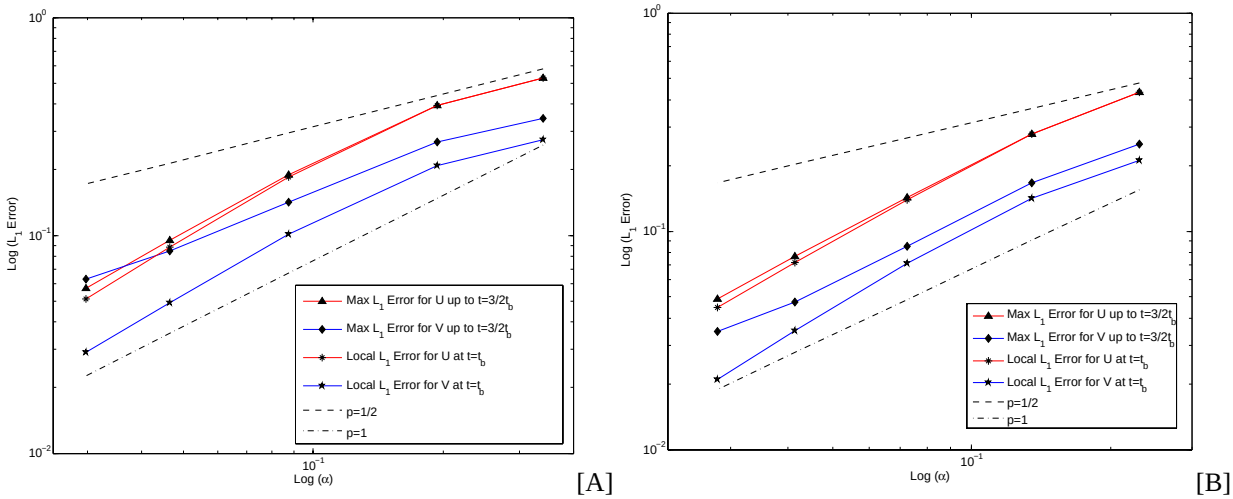

[A] [B]

FIGURE 11. [A]: Relationship between global (max) or local L_1 error and α for $\theta = \frac{2}{3}$ and initial condition $v_o(x) = 1 - Cos(2\pi x)$. [B]:Relationship between global (max) or local L_1 error and α for $\theta = \frac{2}{3}$ and initial condition $v_o = Cos(2\pi x)$. (The reference slope lines are indicated by $p = 1$ and $p = 1/2$.)

Figures 11A and 11B show the relationships between the global error up to $t = \frac{3}{2}t_b$ as well as the local error at t_b as a function of α for both initial conditions (26) and (27) respectively. Both initial conditions demonstrate the same convergence behavior in α. For small α (large N) the order of convergence in α is about 1.2 for local error at $t = t_b$ for both v^α and u^α. The same is true for global error for u^α. However,

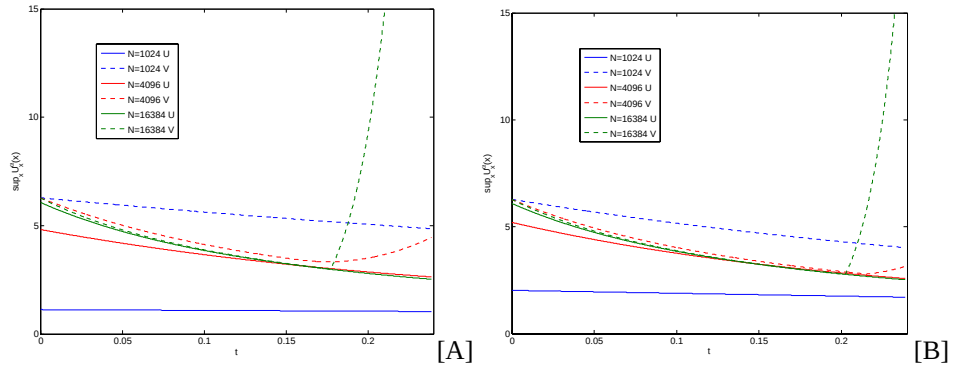

FIGURE 12. Oleinik Inequality (46) plotted for $\theta = \frac{2}{3}$ and initial conditions (26)-[A] and (27)-[B].

the global error for v^α does not seem to settle to a linear profile in log-log scale for small α and instead the order of convergence decreases, implying that v^α does not converge to the exact solution as fast as u^α or perhaps does not converge at all.

To check if the numerically computed solutions satisfy entropy condition, the Oleinik inequality is plotted in Figure 12 for both initial conditions. As in the $\theta = 1$ case, the positive slopes of u^α for $\theta = \frac{2}{3}$ seem to be bounded for both initial conditions, thus implying that the solution appears to satisfy the entropy condition and is physically meaningful. However for v^α the positive slopes become unbounded for larger t causing v^α to violate the entropy condition. Further, as in the $\theta = 1$ case, the rapid growth of v^α_x occurs at earlier times when the mesh is refined.

Both error and entropy investigation imply that it is u^α that appears to converge to the unique entropy solution and not v^α. As it is clearly visible from the plots of the numerical solution for both initial data the oscillations and sharp positive gradients appear around the shock in the case of v^α. This causes the error to grow and results in the violation of the entropy condition for v^α. The function u^α on the other hand is monotone around the region of discontinuity in exact solution and appears to converge steadily without violating the entropy condition.

4.3. $\theta = \frac{1}{3}$. Figures 13 and 14 show the numerical approximations u^α and v^α computed using $\theta = \frac{1}{3}$. It is clear that the solution is well approximated only for regions that are far away from the position of the discontinuity in the exact solution. Oscillations and overshoots develop in both v^α and u^α in this case, and the growth of positive slopes is visible even from the solution curves for as early as $t = t_b$.

The tolerance level $\delta = 10E - 7$ is used with equation (39) to generate a relationship between α and $N = \frac{1}{h}$ computed up to $t = \frac{3}{2}t_b$. This relationship is shown in Figure 15 in log-log scale for both initial

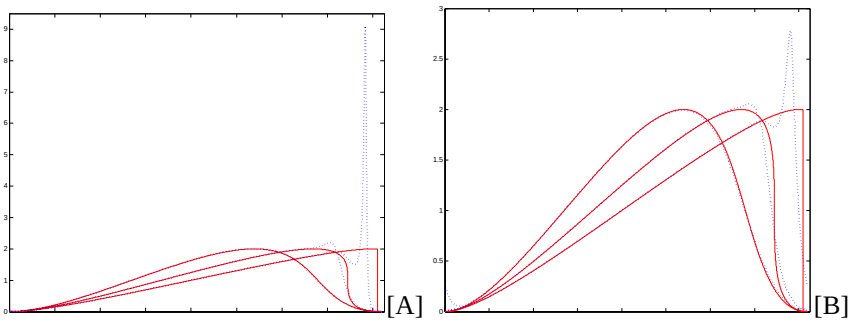
[A] [B]

FIGURE 13. ($\theta = \frac{1}{3}$) Solution curves computed up to $t = \frac{3}{2}t_b$ for the initial data (26). Red solid curves represent the exact solution for $t = (1/2)t_b, t_b, (3/2)t_b$. Blue dotted curves represent the corresponding numerical solution:[A]-$V^\alpha(x)$,[B]-$U^\alpha(x)$.$N = 16384$,$\alpha = 0.0175$.

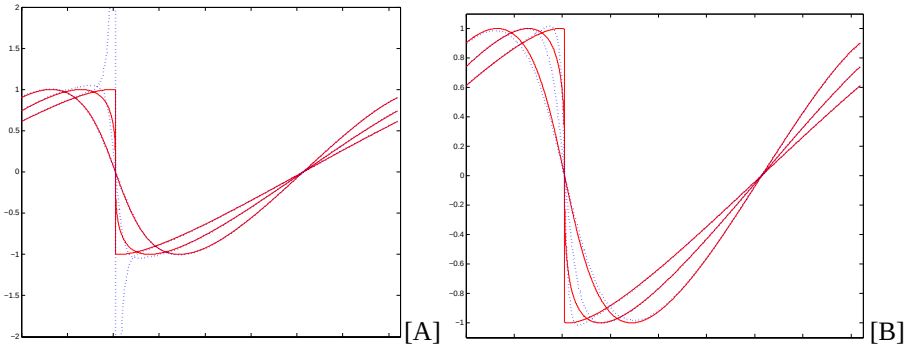
[A] [B]

FIGURE 14. ($\theta = \frac{1}{3}$) Solution curves computed up to $t = \frac{3}{2}t_b$ for the initial data (27). Red solid curves represent the exact solution for $t = (1/2)t_b, t_b, (3/2)t_b$. Blue dotted curves represent the corresponding numerical solution:[A]-$V^\alpha(x)$,[B]-$U^\alpha(x)$.$N = 16384$,$\alpha = 0.0226$.

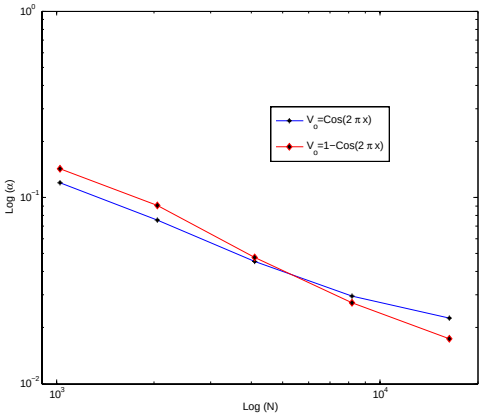

FIGURE 15. Relationship between α and N for $\theta = \frac{1}{3}$ computed up to $\frac{3}{2}$ break time.

conditions (26) and (27). As in the previous cases, the physically meaningful α lie above the curves. For the combinations of α and N below the curves, the modified energy (39) is not conserved in time to the

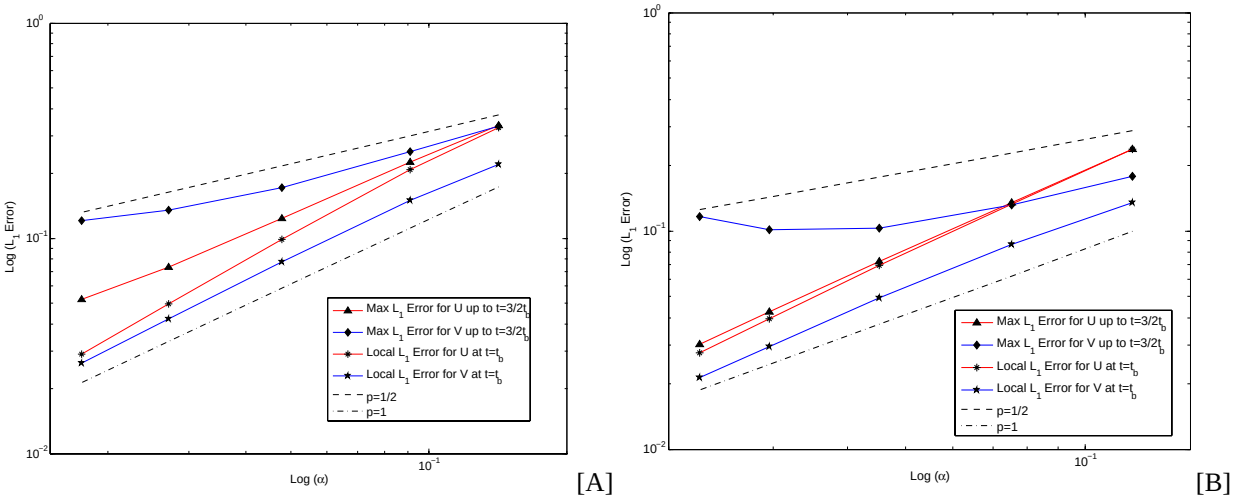

FIGURE 16. [A]: Relationship between global (max) or local L_1 error and α for $\theta = \frac{1}{3}$ and initial condition $v_o(x) = 1 - Cos(2\pi x)$. [B]:Relationship between global (max) or local L_1 error and α for $\theta = \frac{1}{3}$ and initial condition $v_o = Cos(2\pi x)$. (The reference slope lines are indicated by $p = 1$ and $p = 1/2$.)

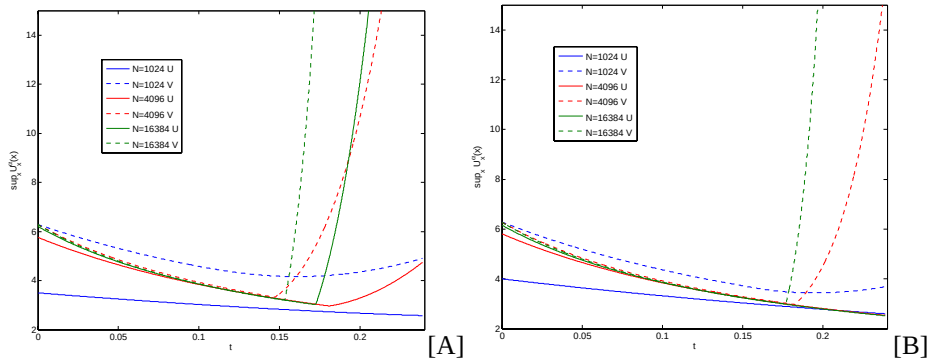

FIGURE 17. Oleinik Inequality (46) plotted for $\theta = \frac{1}{3}$ and initial conditions (26)-[A] and (27)-[B].

tolerance level specified above, thus violating Theorem 3 and therefore not providing an accurate solution to the modeled problem.

Figures 16A and 16B show the relationships between the global and local errors up to $t = \frac{3}{2}t_b$ as a function of α for both initial conditions (26) and (27) respectively. The order of convergence in α for large N of the local L_1 error at break time is about 1.2 for u^α and 1 for v^α for initial conditions (26). For the other initial condition (27) the order is about 1.3 for u^α and 1.2 for v^α. However, the global error, does not appear to settle to a linear loglog profile consistently for both initial data for both u^α and v^α. Thus at the later times after the shock forms in the exact solution, neither v^α nor u^α converges at a constant rate to the exact solution. In fact, the convergence rate in α decreases and the solution apparently diverges.

To check if the numerically computed solutions satisfy the entropy condition, the Oleinik inequality is plotted in Figure 17 for both initial data. Unlike the previous cases of $\theta = 1$ and $\theta = \frac{2}{3}$, the positive slopes of u^α for $\theta = \frac{1}{3}$ also become unbounded, for at least one of the initial conditions (26). This implies that neither u^α nor v^α satisfy the entropy condition and both numerical solutions are not physically meaningful in the limit $h \to 0$.

5. CONCLUSION

We have solved Burgers Equation using the Leray-α regularization numerically using a hybrid algorithm combining finite difference scheme for the conservation law and the spectral method for the regularization. We examined the results for two types of periodic initial data. For both types of initial data considered, shocks form. In one case the shock moves while in the other the shock is stationary. For both initial data and for $\theta = 1$ and $\frac{2}{3}$, we find convergence of the regularized solution u^α to the unique entropy solution of the Burger's Equation. However, v^α was apparently in violation of the entropy condition in all the cases considered. Hence, v^α seemingly does not represent a physically meaningful solution to Burger's equation in the limit $h \to 0$. For $\theta = \frac{1}{3}$ it appears that for the given numerical scheme used, neither u^α nor v^α converge to the unique entropy solution. Further study of this regularization scheme could be done employing different numerical approaches to determine whether there are schemes for which v^α converges to the entropy solution. We conjecture that such schemes are of upwind type and would thus give convergence to the entropy solution even if $\alpha = 0$. Centered difference schemes of the type used here, likely do not have v^α converge to the entropy solution.

6. ACKNOWLEDGEMENTS

The author gratefully acknowledges support from the University of California, Irvine Undergraduate Research Opportunities program. The author also thanks her advisors Professor John Lowengrub and Professor Edriss Titi from the UCI Mathematics Department.

REFERENCES

[1] Knobel, Roger. "An Introduction to Mathematical Theory of Waves." Student Mathematical Library(STML)/IAS/Park City Mathematical Subseries 3 (1999).

[2] LeVeque, Randall. Numerical Methods for Conservation Laws. Basel: Birkhauser Verlag,1992.

[3] Tadmore, Etan, Edriss Titi, and Weigang Zhong. ”A Vanishing Leray-α Model of Burgers Equation.”, (in preparation)

[4] Strikwerda, John. Finite Difference Schemes and Partial Differential Equations. Philadelphia:SIAM,2004.

[5] Thomas, James. Numerical Partial Differential Equations. New York: Springer-Verlag, 1995.

[6] Kifowit,Steve. Fast Fourier Transforms. 8 Jan. 2005 <http://faculty.prairiestate.edu/skifowit/fft>.

[7] Hou, Thomas, John Lowengrub, and Michael Shelley. ”Removing Stiffness from Interfacial Flows with Surface Tension.” Journal of Computational Physics 114(1994): 312-338.

[8] Bhat, Harish. Lagrangian Averaging, Nonlinear Waves and Shock Regularisation. PhD Thesis. Caltech,Pasadena, 2005.

[9] Strauss, Walter. Partial Differential Equations. John Whiley and Sons, 1992.

[10] Iserles, Arieh. A First Course in the Numerical Analysis of Differential Equations. New York: Cambridge University Press, 1996.

[11] Tadmor, Etan. ”Burgers Equation with Vanishing Hyper-Viscosity.” Comm. Mathematical Sciences 2(2004): 317-324

[12] Leray, Jean. ”Sur les movements d’un fluide visqueux remplaissant l’espace.” Acta Mathematica 63(1934): 193.

[13] Krasny, Robert. ”A study of singularity formation in a vortex sheet by the point vortex method.” Journal of Fluid Mechanics 65 (1986): 167.

[14] Boyd, John. Chebyshev and Fourier Spectram Methods. New York: Dover, 2001.

[15] Linshiz, Jasmine, and Edriss Titi. ”Analytical Study of Certain Magnetohydrodynamic-α Models.” Eprintweb. June 1996. <http://arxiv.org/pdf/math/0606603>